 DOI: 10.17344/acsi.2016.2385

Scientific paper

Comparative Photocatalytic Degradation of Monoazo and Diazo Dyes Under Simulated Visible Light Using Fe^{3+}/C/S doped-TiO_2 Nanoparticles

William Wilson Anku,* Samuel Osei-Bonsu Oppong, Sudheesh Kumar Shukla and Poomani Penny Govender*

Department of Applied Chemistry, University of Johannesburg, P.O. Box 17011, Doornfontein 2028, Johannesburg, South Africa.

** Corresponding author: E-mail: pennyg@uj.ac.za, williamanku85@gamil.com Tel:+275596555*

Received: 26-02-2016

Abstract

This research work delved into the photocatalytic degradation of monoazo dye (methyl orange) and diazo dye (congo red) in aqueous solution using Fe^{3+}/C/S-doped TiO_2 nanocomposites. The nanocomposites were synthesised through sol-gel method and characterized using XRD, FTIR, SEM, TEM, EDX, BET and UV-Vis. Photocatalytic degradation of the dyes was monitored under simulated visible light using pristine TiO_2, C/S/doped-TiO_2 and Fe^{3+}/C/S doped-TiO_2 with varying concentrations of Fe^{3+}. The influence of catalyst doping, solution pH, and light intensity were also examined. Doping TiO_2 with Fe^{3+}/C/S caused reduction in its band gap value with the resultant improvement in its visible light activity. The photocatalytic efficiency of the catalysts is given as follows: TiO_2 < C/S/TiO_2 < Fe^{3+}/C/S–TiO_2 with Fe^{3+}/C/S–TiO_2 (0.3% Fe^{3+}) as the best performing photocatalyst. The monoazo dye experienced higher degradation efficiency than the diazo dye. Degradation of the azo dyes was observed to decrease with increasing pH from 2 to 12. Increased visible light intensity enhanced the photodegradation efficiency of the dye. Dye decolourization was observed to be faster than its mineralization.

Keywords: TiO_2, metals, non-metals, azo dyes, photocatalytic degradation, sol-gel method.

1. Introduction

The release of dye polluted wastewater by textile industries into surface water is causing serious environmental challenges. These challenges are not only limited to the aesthetic impact on the water bodies, the negative effect on aquatic plants and death of fish but also the health effects posed to humans, as many of these dyes are toxic and carcinogenic.[1,2]

A large number of dyes with varied chemical structures are used in the textile industries for dyeing purposes. Based on their chemical structures in terms of chromophore groups, dyes can be classified as azo dyes, anthraquinone dyes, and reactive dyes and so on. Azo dyes are the most abundant group of dyes used in the textile industries. The main characteristics of these dyes are the presence of one or more azo (N=N) bonds and bonds between aromatic rings.[3,4] Certain characteristics of dyes such as toxicity, resistance to degradation and photodegradation rates are believed to be dependent on the chemical structure of each dye.[4,5] For example, Giwa et al,[6] investigated the photodegradation of Reactive Yellow 81 and Reactive Violet 1 in aqueous solution with TiO_2–P25 (Degussa) and observed that structural variation between the dyes molecules may have influenced their degradation rates. With regards to aromatic compounds, the number, position and the electronic nature of the substituents determine the efficiency of the photocatalytic degradation process.[7] In their studies to determine the structural effect on photocatalytic degradation of substituted phenols through the use of TiO_2 nanoparticles, Parra et al,[8] observed that photoreactivity of substituted phenol depend on the electronic nature of the substitutes and their positions in the aromatic ring. The photocatalytic degradation process is more effective with greater electronic density on the aromatic ring.[8] Therefore, it necessary to design technologies capable of photode-

grading these dyes with their structural differences in mind.

There has recently been considerable interest in the use of semiconductor photocatalysts for degradation of dyes in wastewater. There has been several reports on the use of TiO_2 to degrade organic compounds in wastewater,[9,10] due to its numerous advantages including high optical, electronic and photocatalytic properties, chemical stability, non-toxicity and low cost.[11] In spite of these advantages, the practical application of TiO_2 as an efficient photocatalyst for complete photodegradation of organic pollutants in wastewater is hampered by some inherent problems associated with TiO_2 as a photocatalyst. These problems include its relatively high band gap of 3.2 eV which limits its ability to work in the visible light range, and its sensitivity to recombination of photogenerated electrons and hole, which decrease its photocatalytic activity.[12]

In order to enhance the photocatalytic activity of TiO_2, its band gap must be reduced, and the recombination rate of the photogenerated electrons and holes minimized. Lots ofeffort has been made into achieving these goals through various modification techniques. One common and most effective method to minimize the electron-hole recombination rate, and extend the absorption edge of TiO_2 from the ultraviolet to visible light region is by doping TiO_2 with transition metal cations.[13,14] Out of many transition metals, iron has been regarded as a suitable dopant. Fe^{3+} has a radius of 0.69 A which is very similar to that of Ti^{4+} (0.75 A). This makes it easier for Fe^{3+} to be easily incorporated into TiO_2 lattice. Furthermore, Fe^{3+} has the potential for trapping photogenerated electrons and holes since the energy level of Fe^{2+}/Fe^{3+} lies close to that of Ti^{3+}/ Ti^{4+}.[15] This subsequently results in improved separation of electron-hole pairs leading to improvement in quantum yield.[16]

Extensive studies have also been undertaken to improve the efficiency of TiO_2 as a photocatalyst through the use of nonmetal dopants such as nitrogen,[17] carbon,[18] sulphur[19] and fluorine.[20] Band gap narrowing has been reported in C, S, and N doped TiO_2,[21,22] with C-doped TiO_2 exhibiting the best band gap narrowing ability.[23] When doped together in TiO_2, the combined effect of charge separation ability of Fe^{3+} and band gap narrowing potential of C and S is envisaged to result in modified TiO_2 with excellent optical and photocatalytic properties.

This work therefore involved the synthesis of pristine TiO_2, C/S-doped TiO_2 and Fe^{3+}/C/S-doped TiO_2 with varying weight percent of Fe^{3+} (0.3%, 0.6% and 1.0%) through the sol-gel method of preparation. The photocatalytic degradation potential of these catalysts was assessed by their degradation of a monoazo dye (methyl orange) and diazo dye (congo red) as a function of time in aqueous solution under simulated visible light. The degradation of these two dyes by the catalysts were compared with regards to their structural differences. The influence of factors such as catalyst modification, pH and visible light intensity on the photocatalytic degradation of the dyes, as well as the degree of mineralization of the dyes was also studied using the catalyst with the best photodegradation potential.

2. Experimental

2. 1. Chemicals and Reagents

Thiourea ($CS(NH_2)_2$), 99% was procured from Hopkin and Williams Ltd., England. Iron (III) chloride hexahydrate ($FeCl_3.6H_2O$), 99% was purchased from Merck, South Africa.The two azo dyes, Congo red and Methyl orange, absolute ethanol and titanium (IV) isopropoxideTi ($OC_3H_7)_4$, 97% were purchased from Sigma Aldrich, Germany.All chemicals used in this work were of analytical grade and were used without any further purification. Double distilled water was used throughout the experiment. The dye standard solutions were prepared by dissolving the appropriate masses of both congo red and methyl orange in 1000 mL. The standard solutions were then diluted to obtain the desired 20 ppm solution of each dye. The structures of the two azo dyes are shown in Figure 1.

2. 2. Synthesis of Fe^{3+}/C/S-doped TiO_2

Titanium (IV) isopropoxide (12.5 mL) was added to 50 mL absolute ethanol, followed by the dropwise addition of 1 mL polyethylene glycol. The mixture was stirred for 30 min. Calculated amounts of iron (III) chloride hexahydrate representing Ti: Fe ratios of 0.3%, 0.6% and 1.0% were dissolved in 2 mL deionized water and added to the mixture. The mixture was stirred for another 1 h.

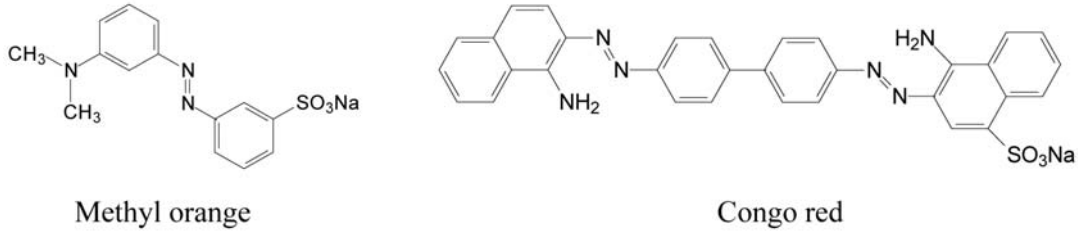

Figure 1. Structure of methyl orange and congo red

Thereafter, 3. 0 g of thiourea, which served as the source of C and S, was dissolved in 10 mL deionized water and added to the mixture slowly with further stirring for another 2 h. Finally, the mixture was dried in an oven at 100 °C for 12 h and calcined at 500 °C for 3 h. The pristine TiO_2 and C/S–TiO_2 were also synthesized following the same procedure but without the addition of both iron (III) chloride hexahydrate and thiourea (in the case of TiO_2), and iron (III) chloride hexahydrate (for C/S–TiO_2).

2. 3. Characterizations

The X-ray diffraction (XRD) pattern was recorded on Philips PANalytical X'pert PRO X-ray diffractometer operating at 40kV using Cu-Kα radiation (λ = 0.1541 nm). The measurement was performed over a diffraction angle range of 2θ = 10°–100°. Fourier transform infrared (FTIR) spectroscopy for the nanocomposites was recorded on PerkinElmer spectrometer (Spectrum 100) in the wavelength range of 400 to 4000 cm^{-1}. The FTIR study was performed by using potassium bromide (KBr) pellet. Scanning electron microscopy (SEM) images were taken with a TESCAN (Vega 3 XMU) instrument. The elemental composition was studied using energy dispersed x-ray (EDX) attached to SEM. Transmission electron microscopy (TEM) images were taken using the TEM microscope (JEOL, JEM-2100F) with a working voltage of 120kV. Investigation of the optical absorption properties was carried out using a UV-Vis spectrophotometer (Shimadzu UV-2450). Barium sulphate ($BaSO_4$) was used as the reflectance standard.

2. 4. Photodegradation Studies of the dye Solutions

The photocatalytic degradation ability of the as synthesized nanoparticles on the two dye solutions was determined by measuring the absorbance of the dye solutions before and after their photodegradation, and the determination of the total organic carbon (TOC) of the dyes solutions before and after their degradation. The simulated visible light intensity was varied using Oriel PV reference cell system model 9115 V to produce a beam power equivalent to 0.5 sun, 0.7 sun, 1.0 sun and 1.3 sun intensities. This was achieved by setting the distance between the solar simulator (equipped with 150W ozone free xenon lamp) and the experimental set up to distances of 15 cm, 13 cm, 10 cm and 0.7 cm respectively. The pHs of the solutions were varied by adding 2M HCl and 2M NaOH solutions and monitored using Orion Per Hect pH meter. A Teledyne Tekmar TOC fusion meter, USA, was used for the total organic carbon analysis.

2. 5. Evaluation of Photocatalytic Activity

The photocatalytic activities of the as-synthesized pristine TiO_2, C/S–TiO_2 and Fe^{3+}/C/S–TiO_2 were probed by their application in the degradation of 20 ppm aqueous solutions of methyl orange and congo red under simulated visible light. In this experiment, 20 mL (20 ppm) solution of each dye was placed in seven 50 mL beakers labelled 0–6. The photocatalysts (0.02 g) were mixed with each of the 7 dye solutions and the mixtures stirred magnetically in the dark for 30 min to establish adsorption equilibrium between the dyes and the catalysts. As a control, the beakers labelled zero (0) were removed after the 30 min stirring without visible light illumination. Then, 5 mL aliquot of this solution was withdrawn using disposable syringes fitted with 0.45 μm PVDF membranes. The remaining solutions labelled 1–6 were then illuminated using a Newport solar simulator, port 9600 full spectrum equipped with 150W ozone free xenon lamp, and fitted with a dichroic UV filter with a wavelength of 420 nm. The illumination was carried out for 180 min. The visible light illuminated solutions were chronologically removed from 1–6 after every 30 min interval and 5 mL aliquot of each was taken. The degradation was performed at the solution pH and 1 sun intensity. The concentrations of the dyes in the withdrawn solution after illumination (5 mL) were determined using Shimadzu UV-2450 spectrophotometer at wavelengths of 497 nm and 462 nm for congo red and methyl orange respectively. The same procedure was followed for the degradation experiments at pHs 3, 7, 9 and 12, and visible light intensities of 0.7 sun, 1.0 sun and 1.3 sun.

3. Results and Discussions

3. 1. FTIR Analysis

The FTIR spectra of the as-synthesized undoped TiO_2, C/S-doped TiO_2 and Fe^{3+}/C/S-doped TiO_2 with varying contents of Fe^{3+} are presented in Figure 2. In all the spectra, the strong and broad band below 1000 cm^{-1} is assigned to the combined bands of Ti–O–Ti, Fe–O–Ti, S–O–Ti and O–Ti–C crystal vibrations,[24] and the absorption bands at 1628 cm^{-1} and around 3500 cm^{-1} are due to –OH bending and stretching vibrations respectively as a result of absorbed water molecules. For the C/S-doped TiO_2 and Fe^{3+}/C/S-doped TiO_2 photocatalysts (Figure 2b, 2c, 2d and 2e), the peak located at 1065 cm^{-1} may be attributed to bidentate sulphate ions (SO_4^{2-}) co-ordinated to metal ions such as T^{4+}.[25] In addition, the peak at 1130 cm^{-1} can be ascribed to the S=O stretching vibration.[26] The small peak at 2048 cm^{-1} may be a consequence of an out-of-phase stretching band of –N=C=O.[27] The spectra for Fe^{3+}/C/S-doped TiO_2 (with varying Fe content) is similar to that of C/S-doped TiO_2 but with changes in relative intensities and peak positions with increasing Fe content. The intensities of the absorption bands for Fe^{3+}/C/S-doped TiO_2 (0.3% Fe^{3+}), (Figure 2c), are comparatively higher than those of the other nanocomposites. This observation is a possible confirmation that the Ti^{4+} is perfectly substituted by Fe^{3+} at this concentration.

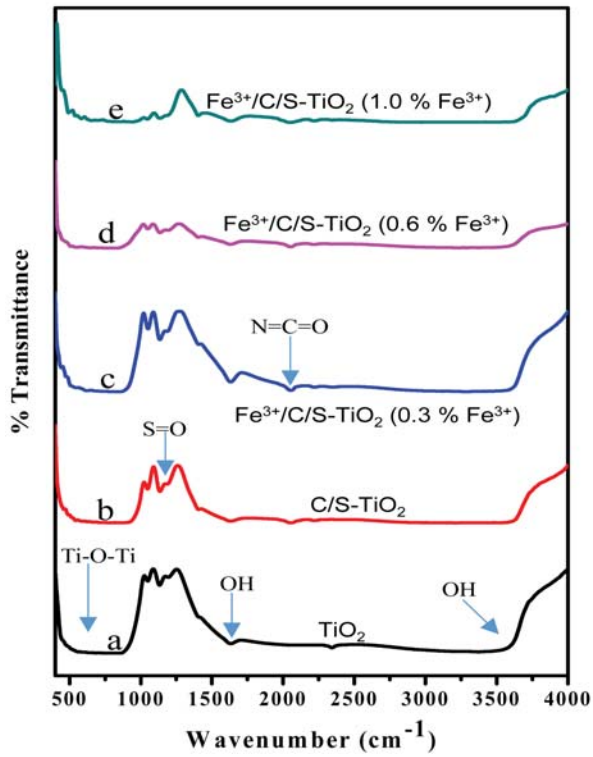

Figure 2. FT-IR spectra of pristine TiO_2, C/S–TiO_2 and Fe^{3+}/C/S-doped TiO_2 with varying concentrations of Fe^{3+}.

3. 2. Powder XRD Analysis

The powder X-Ray diffraction patterns of undoped TiO_2, C/S-doped TiO_2 and Fe^{3+}/C/S-doped TiO_2 are shown in Figure 3. All the diffractions are peaks characteristic of Anatase crystalline phase of TiO_2. These peaks occur at 2θ values of 25.3°, 37.9°, 48.1°, 53.9°, 55.0°, 62.9°, 68.9°, 70.4°, 75.8° and correspond to diffraction planes of 101, 004, 200, 105, 211, 204, 116, 200 and 215 respectively. This diffraction pattern is comparable to JCPDS no_ 21–1272. No Fe containing crystalline phase was observed in the XRD pattern. For a coordinated number of 6, Fe^{3+} and Ti^{4+} have similar ionic radii of 0.65 Å and 0.75 Årespectively. Fe^{3+} can therefore easily substitute Ti^{4+} in the TiO_2 lattice.[28] The result of this analysis therefore means that there was a uniform substitution of Ti^{4+} with Fe^{3+} dopant. It is also evident that the catalysts are small in size due to the broad nature of the peaks. Crystallite sizes of catalysts were calculated using the Debye-Scherrer's equation:[29]

$$D = \frac{K\lambda}{\beta cos\theta} \quad (1)$$

where, D is the crystallite size, K is a shape factor with a value of 0.9, λ is the wavelength of the X-ray (0.1541 nm), β is the value of full width at half maximum (FWHM) in the radiation of (101) plane in 2θ scale, and θ is the Bragg's diffraction angle at the maximum. The crystallite sizes were found to be 23.0 nm, 19.4 nm, 15.7 nm, 12.3 nm and 7.2 nm for TiO_2, C/S-doped TiO_2, Fe^{3+}/C/S-doped TiO_2(0.3% Fe^{3+}), Fe^{3+}/C/S-doped TiO_2 (0.6% Fe^{3+}) and Fe^{3+}/C/S-doped TiO_2 (1.0% Fe^{3+}) respectively. It is evident that doping led to a decrease in the crystallite size of TiO_2 and the size decreased consistently with increasing Fe^{3+} content. This decreased particle size may result in well-defined nanocrystalline powders with high surface area.[30]

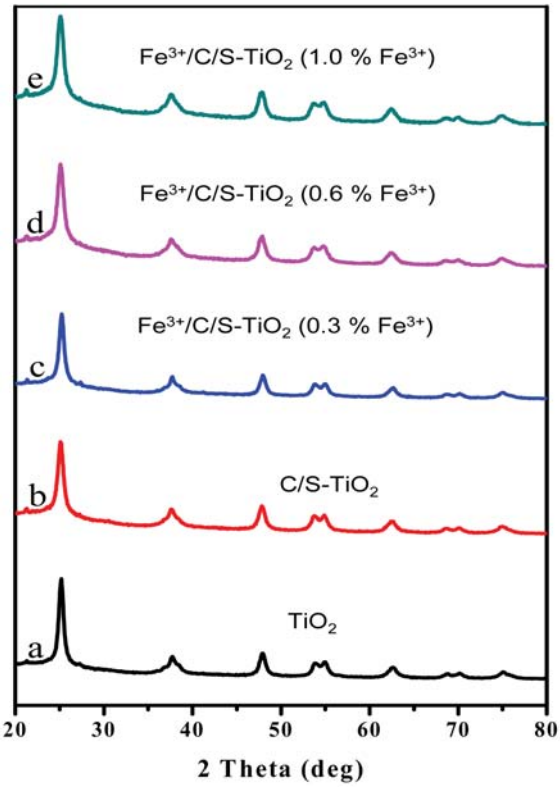

Figure 3 XRD patterns of pristine TiO_2, C/S–TiO_2 and Fe^{3+}/C/S-doped TiO_2 with varying concentrations of Fe^{3+}.

3. 3. Brunauer-Emmett-Teller (BET) Surface Area Analysis

The surface area analysis was intended to provide specific surface area assessment of the nanoparticles. Nitrogen adsorption-desorption isotherm was used to establish the effect of Fe doping on the BET surface, pore volumes and pore sizes of the nanoparticles. The results of the BET surface area, pore volume, and pore size analysis are presented in Table 1. The result shows that the nanocomposites exhibited increased surface area with decreased crystallite size. Thus the undoped TiO_2 had the least surface area of 32.7 m^2/g while the Fe^{3+}/C/S-doped TiO_2 (0.3% Fe^{3+}) had the largest specific surface area of 74.6 m^2/g. Larger surface area can result in improved photocatalytic

Table 1 Surface area, pore volume, pore size, indirect band gap, and percent degradation based on catalyst doping at solution pH and visible light irradiation with 1 sun intensity

Sample	Surface area (m^2/g)	Pore volume (cmg^{-1})	Pore size (nm)	Indirect band gap (eV)	% Degradation	
					Methyl Orange	Congo Red
TiO_2	32.7	0.137	3.825	3.20	32.5	15.2
C/S–TiO_2	32.5	0.180	3.794	2.42	69.4	61.9
Fe^{3+}/C/S–TiO_2 (0.3% Fe^{3+})	74.3	0.212	3.775	2.00	93.5	87.9
Fe^{3+}/C/S–TiO_2 (0.6% Fe^{3+})	56.1	0.224	3.719	2.14	90.7	83.0
Fe^{3+}/C/S–TiO_2 (1.0% Fe^{3+})	44.6	0.233	3.667	2.26	86.4	80.0

property as a result of availability of more active surface sites for improved adsorption of dye molecules.[31] In addition, the pore volumes increase while the pore sizes decrease with increasing Fe concentration. Thus doping TiO_2 with Fe ensured nanoparticles with larger surface area and pore volumes, and reduced pore sizes.

3. 4. SEM, TEM and EDX Analysis

The surface morphology, microstructure and elemental compositions of the as-synthesized nanoparticles were investigated using scanning electron microscopy (SEM), transmission electron microscopy (TEM) and energy dis-

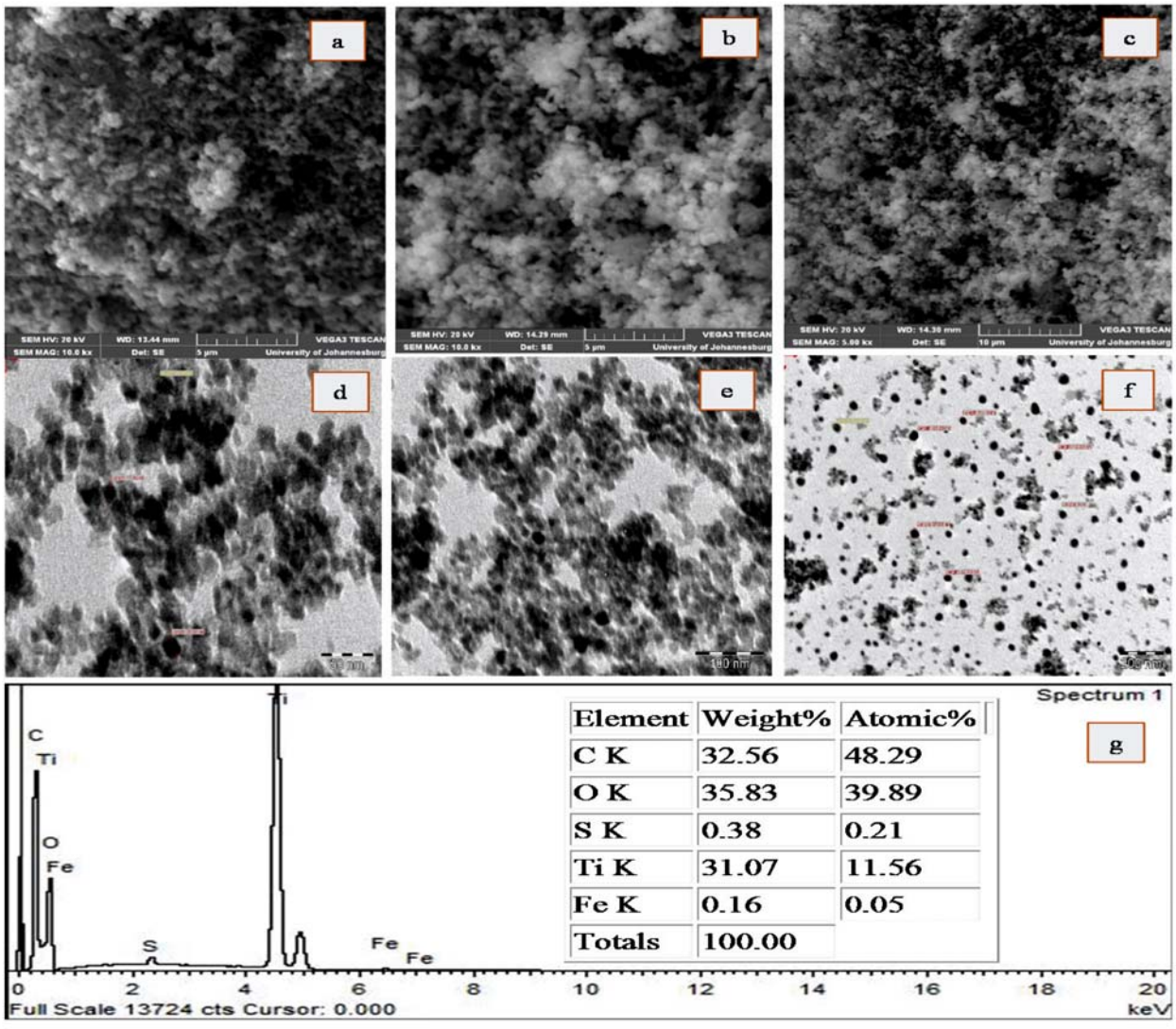

Figure 4 (a) SEM image TiO_2 (b) SEM image C/S–TiO_2 (c) SEM image of Fe^{3+}/C/S-doped TiO_2 (1.0% Fe^{3+}) (d) TEM image of TiO_2 (e) TEM image of C/S–TiO_2 (f) TEM image of Fe^{3+}/C/S-doped TiO_2 (1.0% Fe^{3+}) and (g) EDX spectrum of Fe^{3+}/C/S-doped TiO_2 (1.0% Fe^{3+})

persive X-ray (EDX) respectively. The SEM images of TiO_2, C/S–TiO_2, Fe^{3+}/C/S-doped TiO_2 (1.0% Fe^{3+}) (Figure 4a, 4b and 4c) respectively, and the TEM images of TiO_2, C/S–TiO_2 and Fe^{3+}/C/S–TiO_2 (1.0% Fe^{3+}) (Figure 4d, 4e and 4f) respectively revealed the crystalline and small-sized nature of the catalysts with distinct boundaries. Some aggregation of the nanoparticles was however observed. The EDX spectrum of Fe^{3+}/C/S-doped TiO_2 (1.0% Fe^{3+}) nanoparticle is shown in (Figure 4g). The EDX spectrum confirmed Ti, O, Fe, C and S as the components of the synthesized catalyst. The result shows strong peaks for Ti, O, and C.

3. 5. UV-Vis Analysis

The UV-Vis absorption spectra of pure TiO_2, C/S–TiO_2 and Fe^{3+}/C/S–TiO_2 with varying wt% of Fe^{3+} is displayed in Figure 5. A significant red shift in the absorption spectrum of the pure TiO_2 with the introduction of Fe, C and S can be observed. The absorption edge of the pure TiO_2 occurred below 400 nm, meaning that its light absorption is limited only to the UV light range. However, the absorption edge significantly shifted to around 500 nm with the addition of the dopants. This is an indication that doping of pure TiO_2 with C, S, and Fe improved its visible light absorption ability. This occurrence can be explained in terms of quantum confinement effect. It is observable that Fe^{3+}/C/S–TiO_2 (0.3% Fe^{3+}), (Figure 5c) showed the highest absorption in the visible light region. The characteristic absorption band around 300 nm is a phenomenon attributed to inter band (valence and conduction band) and excitonic transition.[27]

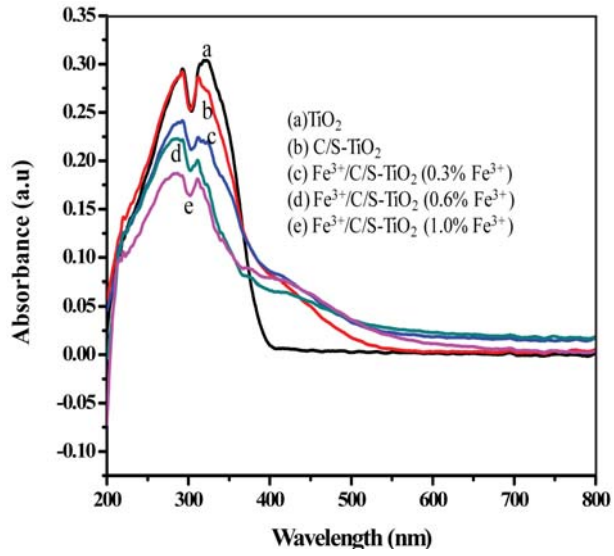

Figure 5. UV-Vis spectra of TiO_2, C/S-doped TiO_2 and Fe^{3+}/C/S-doped TiO_2 with varying concentrations of Fe^{3+}.

3. 6. Band Gap Analysis

The band gap values of the photocatalysts were obtained from a plot of Kubelka-Munk function through the

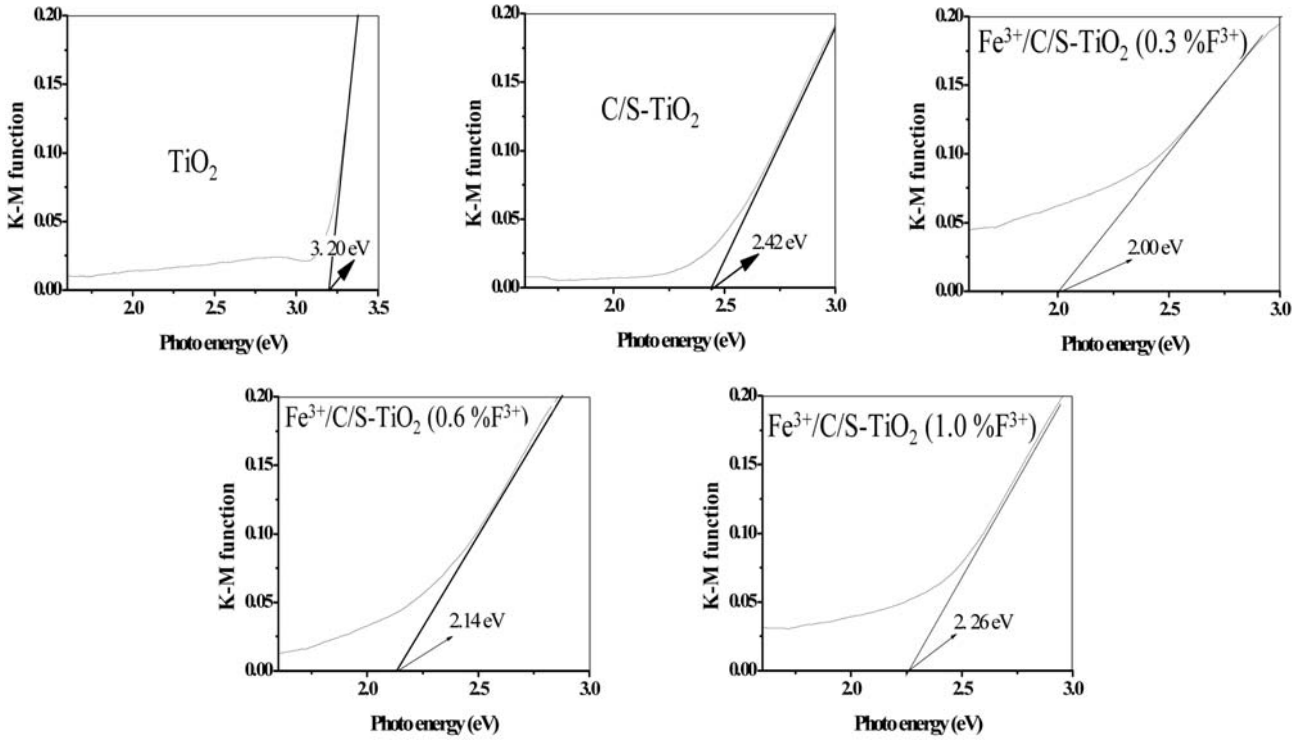

Figure 6 Tauc plot for pure TiO_2, C/S-doped TiO_2 and Fe^{3+}/C/S-doped TiO_2 with varying concentrations of Fe^{3+}.

use of reflectance data. The Kubelka-Munk function is given in equation 4 below:

$$F(R) = \frac{(1-R)}{2R} \quad (2)$$

where, the reflectance (R) = $R_{sample}/R_{reference}$. The Tauc plots for the pure and modified TiO_2 which were obtained by plotting Tauc function (Š(F(R)*híĆ^n against photo energy (hí) with n = 2, are depicted in Figure 6. The band gap values of the various catalysts are presented in Table 1. According to the results, the Fe^{3+}/C/S–TiO_2 (0.3% Fe^{3+}) has the smallest band gap value of 2.00 eV while pure TiO_2 has the highest value of 3.20 eV. This observation clearly verifies that doping of TiO_2 with Fe/C and S successfully reduced its band gap. The band gap values decrease in the following order: Fe^{3+}/C/S–TiO_2 (0.3% Fe^{3+}) < Fe^{3+}/C/S–TiO_2 (0.6% Fe^{3+}) < Fe^{3+}/C/S–TiO_2 (1.0% Fe^{3+}) < C/S–TiO_2 < TiO_2. Band gap narrowing can allow more absorption of visible light, and narrower band gap leads to more visible light absorption.[32,33] It is however important to note that after the 0.3% Fe^{3+} dopant concentration the band gap values increase consistently with an increase in Fe^{3+} concentration. Such observation has been attributed to the steady movement of the conduction band of TiO_2 above the first excited state of the dopant ion due to the increased dopant concentration. The dopant ions at the first excited state interact with the conduction band electrons of TiO_2 causing higher energy transfer from the TiO_2 to the metal dopant ions[34] In addition, increase in band gap value with increased dopant concentration could be ascribed to increase in n-type carrier concentration as the absorption edge shifts to higher energy level.[35]

3. 7. Photodegradation Analysis

According to Harikumar et al.[36] it is necessary to understand the reaction rate and the manner in which the rate is affected by different factors in in order to design an optimized photodegradation system. Photocatalytic degradation process depends on many factors such as such as pH, light intensity, type of catalyst, oxygen concentration, concentration of the pollutant and the presence of inorganic ions. In this study, the degradation efficiencies of the dyes were studied based on catalyst type (effect of doping), light intensity and pH.

3. 7. 1. Effect of Doping

The photodegradation ability of the as-synthesized photocatalysts (TiO_2, C/S–TiO_2, Fe^{3+}/C/S–TiO_2 (0.3% Fe^{3+}), Fe^{3+}/C/S–TiO_2 (0.6% Fe^{3+}) and Fe^{3+}/C/S–TiO_2 (1.0% Fe^{3+}) was tested by applying them in the degradation of 20 mL (20 ppm) solution of methyl orange (monoazo dye) and congo red (diazo dye) with 0.02g of each catalyst. This experiment was carried out under simulated visible light intensity of 1 sun for 180 min. In addition, the degradation experiment was performed using bare TiO_2 in the absence of UV filter. This was intended to find out the influence of UV filter on photocatalytic performance of TiO_2. Bank experiment (without catalyst) was also performed. The result for methyl orange degradation is shown in Figure 7 (A) while that of congo red is presented in Figure 7 (B). It is apparent that the photodegradation efficiency of all the catalysts against both methyl orange and congo red exhibited the same trend where Fe^{3+}/C/S–TiO_2 (0.3% Fe^{3+}) exhibited the best degradation efficiency against both dyes while TiO_2 displayed the least degradation efficiency for both dyes. The rest of the catalysts degraded both dyes in the following order: C/S–TiO_2 < Fe^{3+}/C/S–TiO_2 (1.0% Fe^{3+}) < Fe^{3+}/C/S–TiO_2 (0.6% Fe^{3+}). Compared to the use of UV filter, the bare TiO_2 demonstrated higher photocatalytic degradation efficiency against both dyes in the absence of UV filter. This means that, though not to an appreciable extent, the unmodified TiO_2 is relatively efficient in the UV range compared to the visible light range. However, the presence of the dopants extent it's activity to the visible light range, resulting in higher degradation efficiency of the modified TiO_2 samples. The bank test indicated that photolysis of both dyes was very slow. The percentage degradation of both dyes by each catalyst is presented in Table 1. The enhanced photocatalytic activity of Fe^{3+}/C/S–TiO_2 (0.3% Fe^{3+}) compared to other catalysts can be attributed to its improved visible light absorption (Figure 5), larger surface area, and reduced bad gap (Table 1). These factors possibly resulted in improved utilization of visible light instead of UV light, charge carrier transfer efficiency, enhanced adsorption of dye molecules and subsequent photodegradation due to large surface area and retardation of electron-hole recombination emanating from acceptance of electrons from the conduction band by the dopant ions.

It is obvious, by comparing Figure 7 (A and B); that the monoazo dye was degraded faster than the diazo dye. All the catalysts demonstrated higher photodegradation of the monoazo dye compared to the diazo dye. For example, the best photocatalyst, Fe^{3+}/C/S–TiO_2 (0.3% Fe^{3+}), degraded about 93% of methyl orange within 180 min (Figure 7A) while about 87% of congo red was degraded by the same catalyst within the same time frame (Figure 7B). This difference in photodegradation efficiency of the two azo dyes can be ascribed to structural differences. According to Figure 1, methyl orange contains one azo bond and one sulphonic group while congo red contain two azo bonds and two sulphonic groups. Meanwhile, the degradation of azo dyes is initiated by the electrophilic cleavage of its chromophoric azo bond (–N=N–) attached to the naphthalene ring.[37] Thus the more azo bonds there are in the structure of the dye the longer time it will take to degrade the dye. In addition, azo dyes colour removal and degradation rates have been observed to be proportional to the number of azo and sulphonic groups present in their

molecules.[9] It can therefore be proposed that there exist a direct relationship between the dyes degradation efficiency and the number of azo bonds and sulphonic groups available in the dye molecules.

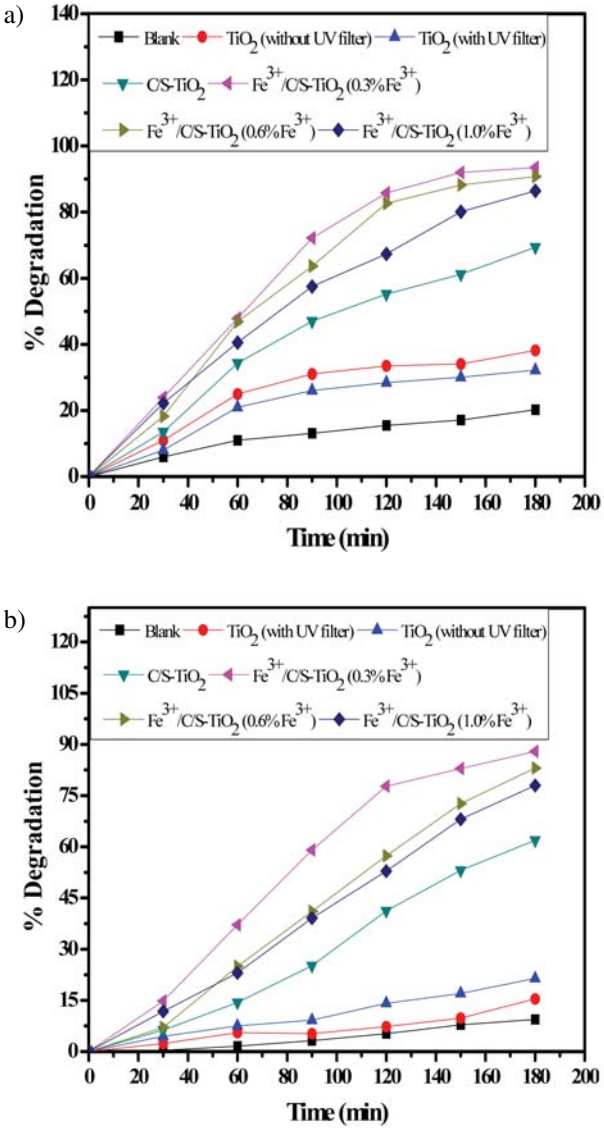

Figure 7. Effect of catalyst doping on degradation efficiency of (A) methyl orange and (B) Congo red by TiO_2, C/S-doped TiO_2 and Fe^{3+}/C/S-doped TiO_2 with varying concentrations of Fe^{3+}.

In order to confirm the proposition that degradation efficiencies of the dyes were influenced by the azo bonds and sulphonic groups present in their molecules, photocatalytic degradation of a 20 mL (20 ppm) triazo dye (Direct blue 71) was further performed using 0.02 g of Fe^{3+}/C/S–TiO_2 (0.3% Fe^{3+}) for 180 min. This compound has three azo bonds and four sulphonic groups. The result (Figure 8) show that the dye experienced 62.8% degradation efficiency. Compared to the degradation efficiencies of methyl orange (93.5%) and Congo red (87.9%), direct blue 71 was degraded at a comparatively lower rate. This observation confirms the proposed direct relationship between the dyes degradation efficiency and the number of azo bonds and sulphonic groups available in dye molecules.

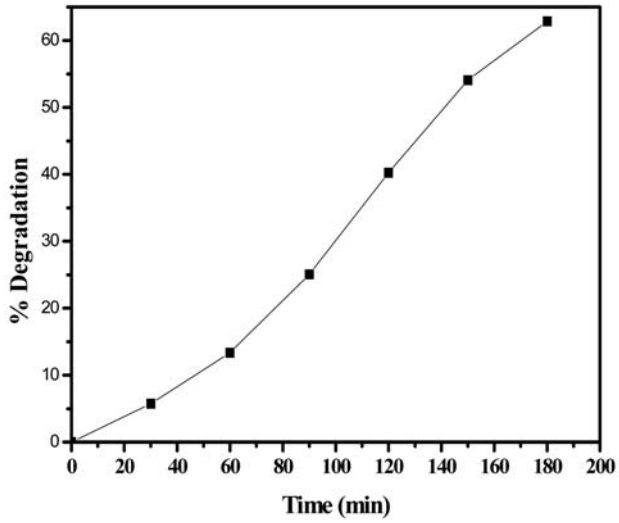

Figure 8. Degradation efficiency of direct blue 71 by of Fe^{3+}/C/S–TiO_2 (0.3% Fe^{3+}

Pseudo-first-order kinetics (Eqn 5) was used to determine the rate of degradation of the dyes by the various catalysts.

$$\ln \frac{Co}{Ct} = k(t) \qquad (3)$$

where C_o is the initial concentration, C_t is the time t and k is the rate constant.

The results are presented in Figure 9 (A and B) for methyl orange and Congo red degradation rates respectively. The result show that the two dyes were degraded at different rates by all the catalysts. Fe^{3+}/C/S–TiO_2 (0.3% Fe^{3+} (the best photocatalyst) degraded both methyl orange and Congo red at faster rates of 16.28×10^{-3} and 15.33×10^{-3} while the bare TiO_2 degraded both dyes at the lowest rates of 2.66×10^{-3} and 1.80×10^{-3} respectively. Comparatively, methyl orange experienced faster rate of degradation than Congo red.

Because of its higher photocatalytic degradation efficiency against the two azo dyes, Fe^{3+}/C/S–TiO_2 (0.3% Fe^{3+}) was the catalyst used to study the effects of light intensity and pH on the degradation efficiency of azo dyes. In addition, because methyl orange was degraded faster, it was chosen as a representative azo dye to study the effect of light intensity and pH on photodegradation of azo dyes.

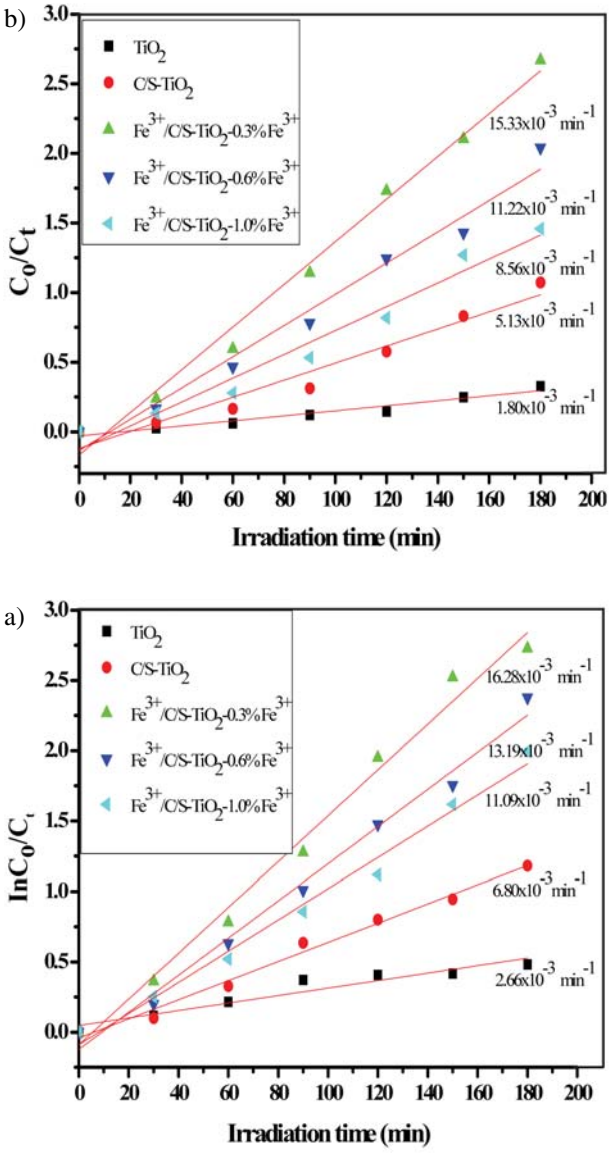

Figure 9. Kinetics of (A) methyl orange degradation and (B) Congo red degradation by TiO_2, C/S-doped TiO_2 and Fe^{3+}/C/S-doped TiO_2 with varying concentrations of Fe^{3+} under visible light irradiation.

3. 7. 2. Effect of pH

One of the major factors that affect the degradation of pollutants by semiconductor photocatalyst is the solution pH since the catalyst surface charge and isoelectric point depend on pH. In addition, the solution pH is also a factor that determines the charge on the dye molecule. The study of the effect of pH on the photocatalytic degradation of organic pollutant is therefore an important consideration. In this study, the effect of pH on azo dye degradation was performed in the range of 2 to 12 with 0.02g of Fe^{3+}/C/S–TiO_2 (0.3% Fe^{3+}) photocatalyst dispersed in 20 mL (20 ppm) solution of methyl orange. The results are displayed in Figure 10. The result showed that the photodegradation efficiency of methyl orange decreased consistently with increasing pH from pH 2 to 12. There are many factors that determine the effect of pH on dye photocatalytic degradation process, amongst which is the acid-base property of the photocatalyst which can be explained in terms of zero point charge,[38] and the fact that the ionization state of the dye molecule depends on the solution pH. TiO_2 has a zero point charge (pH pzc) at pH 6.8. This means that at pH < 6.8 (acidic medium) the surface of TiO_2 becomes positively charged, and negatively charged in alkaline medium (pH > 6.8).[36,39] On the other hand, due to its sulfonic group (SO_3^-), methyl organge is negatively charged in solution. Hence there exist electrostatic force of attraction between the positively charged TiO_2 surface and the negatively charged sulfonic groups of methyl orange in acidic medium. Consequently, the dye molecules were strongly adsorbed onto the TiO_2 surface resulting in efficient degradation of the dye in acidic medium. In the alkaline medium however, both the TiO_2 surface and the dye molecules are negatively charged resulting in electrostatic repulsion of the dye molecules. This caused the dye molecules to be sparingly adsorbed on the TiO_2 surface resulting in diminished degradation efficiency of the dye in alkaline medium. The result therefore indicates that the degradation efficiency of the dye depends on the amount of dye molecule adsorbed onto the TiO_2 surface.

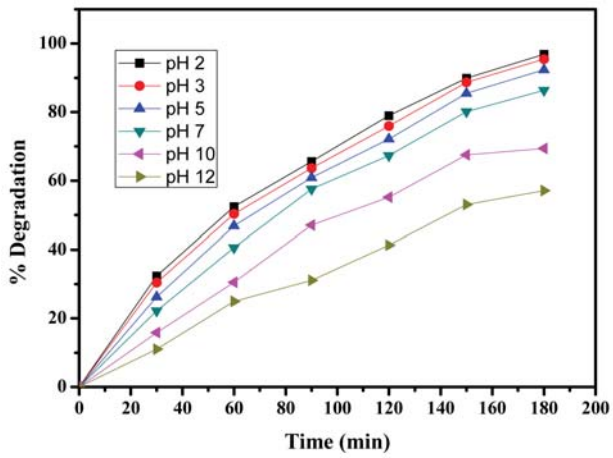

Figure 10. Effect of pH on degradation efficiency of methyl orange by Fe^{3+}/C/S-doped TiO_2 (0.3% Fe^{3+}) nanoparticle.

3. 7. 3. Effect of Light Intensity

Photodegradation of methyl orange solutions under varied visible light intensities, 0.5 sun, 0.7 sun, 1.0 sun and 1.3 sun intensities, was performed to determine the influence of light intensity on the degradation efficiencies of the dye. Oriel PV reference cell system, model 91150V, was used to measure the irradiance of the simulated sun. This experiment was performed with the same catalyst

and dye solution specifications of 0.02 g catalyst suspended in 20 mL (20 ppm) solutions within an irradiation time of 180 min. Figure 11 represents the outcome of this analysis. There was a direct relationship between visible light intensity and degradation efficiency of the dye with respect to 0.5 sun, 0.7 sun and 1.0 sun. There was minimal degradation of the dye at 0.5 sun and 0.7 sun intensity while higher degradation was observed at 1.0 sun intensity to the point that about 93% of the dye was degraded within 120 min. Meanwhile, about 36% and 55% of the dye were degraded within the same 120 min at 0.5 sun and 0.7 sun intensities respectively. This occurrence may be related to the increase in light intensity resulting in an increase of the number of photons that reach the surface of the catalyst. As a result, the number of exited catalyst molecules increase causing an increase in the number of hydroxyl and superoxide radicals responsible for the photodegradation process. On the other hand, an increase in light intensity to 1.3 sun did not result in any significant corresponding increase in the degradation efficiency. This probably means that the optimum number of photons required for an effective photocatalytic degradation was attained at 1.0 sun. Therefore, an increase in photon number at 1.3 sun did not produce any major change in the degradation efficiency.

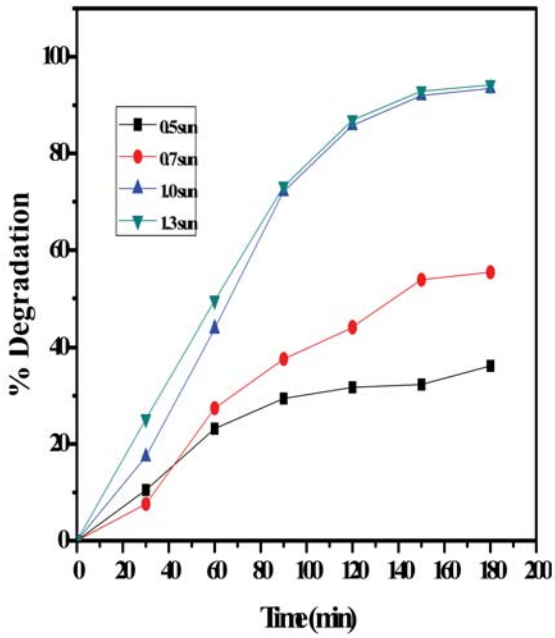

Figure 11. Effect of light intensity on degradation efficiency of methyl orange by Fe^{3+}/C/S-doped TiO_2 (0.3% Fe^{3+}) nanoparticle.

3. 7. 4. Total Organic Carbon Analysis

Total organic carbon (TOC) analysis was performed in order to determine the extent of mineralization of the methyl orange attained during the photodegradation process. This analysis is necessary because the disappearance of dye colour alone cannot be used as a measure to determine complete mineralization of the dye. Furthermore, the photodegradation process can result in the formation of colourless dye intermediates resulting in the disappearance of colour but may actually be more toxic than the dye itself. The analysis was done on the sample irradiated with 1 sun intensity with Fe^{3+}/C/S–TiO_2 (0.3% Fe^{3+}) nanoparticle. The result of this analysis (Figure 12) revealed that the colour disappearance of the dye was faster than the degree of mineralization. The highest TOC removal was around 65%. The quick disappearance of colour could arise from the cleavage of the azo bond while the high TOC value may be due to difficulty in converting the N atom of the dye into oxidized nitrogen compounds since the hydroxyl radicals are short-lived and aliphatic chain interaction with hydroxyl radicals is minimal.[40] This could mean that the dye molecules were converted to other intermediate forms which still exist in the solution irrespective of the dye decolourization, and signifies that degradation of the dye beyond 180 min may lead to complete mineralization.

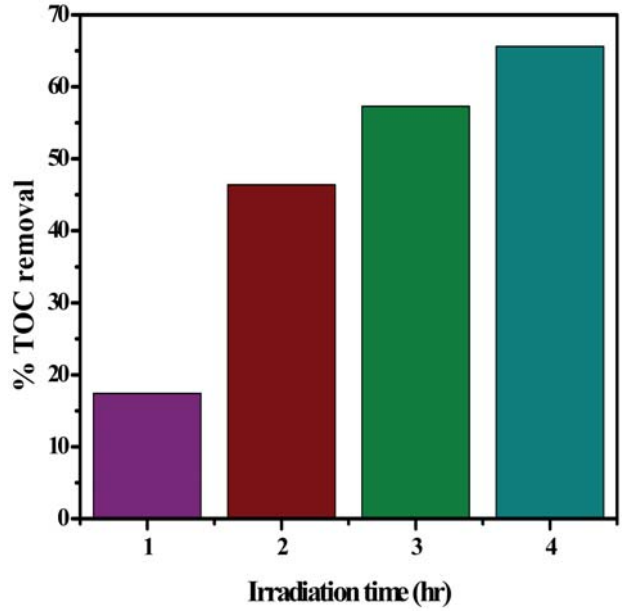

Figure 12. Percent TOC removal by Fe^{3+}/C/S–TiO_2 (0.3% Fe^{3+}) nanoparticle.

4. Conclusion

The visible light active hetero-elements doped TiO_2 was successfully synthesized through sol-gel method, confirmed by FTIR, XRD, EDX AND UV-Vis analyses. Fe^{3+}/C/S–TiO_2 (0.3% Fe^{3+}) was observed to be the best photocatalyst for the degradation of the azo dyes. The enhanced photocatalytic activity of Fe^{3+}/C/S–TiO_2 (0.3%

Fe^{3+}) compared to other catalysts can be attributed to its improved visible light absorption, larger surface area, and reduced bad gap. These factors possibly resulted in improved utilization of visible light, enhanced charge carrier transfer efficiency, greater adsorption of dye molecules and subsequent effective photodegradation of the dye. The monoazo dye experienced higher degradation efficiency over the diazo dye. The fast photodegradation of the monoazo dye compared to the diazo dye indicates that the number of azo bonds and sulphonic groups present in the azo dyes determined their photodegradation rate. The result of pH analysis showed that the photodegradation efficiency of methyl orange decreased consistently with increasing pH from 2 to 12 indicating that the degradation efficiency of the dye depend on the amount of dye molecule adsorbed on the TiO_2 surface. There was a direct relationship between visible light intensity and degradation efficiency of the dye. TOC analysis revealed incomplete mineralization of the dye molecules within 180 min irrespective of the dye decolourization thus signifying that degradation of the dye beyond 180 min may lead to complete mineralization.

5. Reference

1. B. Manu, S. Chaudhari, *Bioresour. Technol*. **2002**, *82*, 225–231. http://dx.doi.org/10.1016/S0960-8524(01)00190-0
2. N. D. Lourenço, J. M. Novais, H. M. Pinheiro, *Environ technol*. **2003**, *24*, 679–686. http://dx.doi.org/10.1080/09593330309385603
3. H. Zollinger. Color chemistry – Synthesis, properties, and applications of organic dyes and pigments, Willey-VCH: New York, **2003**, pp. 219–243.
4. M. C. Costa, F. S. B. Mota, A. B. D. Santos, G. L. F. Mendonça, R. F. D. Nascimento, *Quím. Nova*, **2012**, *35*, 482–486. http://dx.doi.org/10.1590/S0100-40422012000300008
5. Y. H. Lee, S. G. Pavlostathis, *Water Res*. **2004**, *38*, 1838–1852. http://dx.doi.org/10.1016/j.watres.2003.12.028
6. A. Giwa, P. O. Nkeonye, K. A. Bello, E. G. Kolawole, A. O. Campos, *Int. J. App*, **2012**, *2*.
7. S. Parra, J. Olivero, C. Pulgarin, *Appl. Catal. Part B: Environ*. **2002**, 36, 75–85. http://dx.doi.org/10.1016/S0926-3373(01)00283-1
8. S. Parra, J. Olivero, L. Pacheco, C. Pulgarin. *Catal. Part B: Environ. **2003*** 43, 293–301.
9. S. A. Abo-Farha, *J.Am. Sci*, **2010***,* *6*, 130–142.
10. U. G. Akpan, B. H. Hameed, *J. Hazard. Mater*, **2009**,*170*, 520–529. http://dx.doi.org/10.1016/j.jhazmat.2009.05.039
11. X. Zhang, Y. Wang, G. Li, *J Mol. Catal A-Chem*. **2005**, *237*, 199–205. http://dx.doi.org/10.1016/j.molcata.2005.03.043
12. B. Tryba, *Int. J. Photoenergy*, **2008**, *2008*.
13. C. Adán, A. Bahamonde, M. Fernández-García, A. Martínez-Arias*, Appl. Catal B: Environ*. **2007**, *72*, 11–17. http://dx.doi.org/10.1016/j.apcatb.2006.09.018
14. A. K. Ghosh, H. P. Maruska, *J. Electrochem. Soc*. **1977**, *124*, 1516–1522. http://dx.doi.org/10.1149/1.2133104
15. W. Choi, A. Termin, M. R. Hoffmann, *J. Phys. Chem*, **1994**, *98*, 13669–13679. http://dx.doi.org/10.1021/j100102a038
16. N. Riaz, B. K. Mohamad Azmi, A. M. Shariff, *Adv. Mat. Res*. **2014**, *925*, 689–693. http://dx.doi.org/10.4028/www.scientific.net/AMR.925.689
17. R. Y. O. J. I. Asahi, T. A. K. E. S. H. I.Morikawa, T. Ohwaki, K. Aoki, Y. Taga, *Science*, **2001**, *293*, 269–271. http://dx.doi.org/10.1126/science.1061051
18. S. Sakthivel, H. Kisch, *Angew. Chem. Int. Ed*. **2003**, *42*, 4908–4911. http://dx.doi.org/10.1002/anie.200351577
19. T. Umebayashi, T. Yamaki, H. Itoh, K. Asai, *Appl. Phys. Lett*. **2002**, *81*, 454–456. http://dx.doi.org/10.1063/1.1493647
20. J. C. Yu, J. Yu, W. Ho, Z. Jiang, L. Zhang, *Chem. Mater*. **2002**, *14*, 3808–3816. http://dx.doi.org/10.1021/cm020027c
21. D. E. De Vos, M. Dams, B. F. Sels, P. A. Jacobs, *Chem Rev*, **2002**, *102*, 3615–3640. http://dx.doi.org/10.1021/cr010368u
22. E. Barborini, A. M. Conti, I. Kholmanov, P. Piseri, A. Podestà, P. Milani, M. Sancrotti, *Adv. Mater*, **2005**, *17*, 1842–1846. http://dx.doi.org/10.1002/adma.200401169
23. J. C. Yu, W. Ho, J. Yu, H. Yip, P. K. Wong, J. Zhao, *Environ. Sci. Technol*, **2005**, *39*, 1175–1179. http://dx.doi.org/10.1021/es035374h
24. V. Etacheri, M. K. Seery, S. J. Hinder, S. C. Pillai, *Chem. Mater*, **2010**, *22*, 3843–3853. http://dx.doi.org/10.1021/cm903260f
25. F. Wei, L. Ni, P. Cui, *J. Hazard. Mater*. **2008**, *156*, 135–140. http://dx.doi.org/10.1016/j.jhazmat.2007.12.018
26. B. Liang, L Andrews, *J. Phys. Chem A*, **2002**, *106*, 6945–6951. http://dx.doi.org/10.1021/jp025915+
27. L. Ren, X. Huang, F. Sun, X. He, *Mater lett*, **2007**, *61*, 427–431. http://dx.doi.org/10.1016/j.matlet.2006.04.097
28. J. Zhu, W. Zheng, B. He, J. Zhang, M. Anpo, *J. Mol. Catal A*: *Chem*. **2004**, *216*, 35–43. http://dx.doi.org/10.1016/j.molcata.2004.01.008
29. A. K. Singh, U. T. Nakate, *Sci. World J*. **2014**, *2014*.
30. J. Moon, H. Takagi, Y. Fujishiro, M. Awano, *J. Mater. Sci*. **2001**, *36*, 949–955. http://dx.doi.org/10.1023/A:1004819706292
31. J. Moon, H. Takagi, Y. Fujishiro, M. Awano, *J. Mater. Sci*, **2001**, *36*, 949–955. http://dx.doi.org/10.1023/A:1004819706292
32. M. Xing, X. Li, J. Zhang. *Sci. Rep*. **2014**, *4*, 1–7.
33. K. Maeda, K. Domen. *J. Phys. Chem. Lett*. **2010**, *1*, 2655–2661. http://dx.doi.org/10.1021/jz1007966
34. S. Kumar, Z. Jindal, N. Kumari, N. K. Verma. J Nanopart. Res. **2011**, *13*, 5465–5471. http://dx.doi.org/10.1007/s11051-011-0534-5
35. S. A. Yousaf, S. Ali. *Coden. Jnsmac*. **2008**, *48*, 43–50.
36. P. S. Harikumar, L. Joseph, A. Dhanya, *J. Environ. Eng. Ecol. Sci*. **2013**, *2*, 2. http://dx.doi.org/10.7243/2050-1323-2-2
37. M. Muruganandham, M. Swaminathan, *Dyes Pigm*. **2004**, *62*, 269–275. http://dx.doi.org/10.1016/j.dyepig.2003.12.006

38. H. R. Pouretedal, M. Hosseini, *Acta Chim. Slov*, **2010**, *57*, 415–423.
39. N. Wang, J. Li, L. Zhu, Y. Dong, H. Tang, H. *J. Photochem. Photobiol A: Chem.* **2008**, *198*, 282–287. http://dx.doi.org/10.1016/j.jphotochem.2008.03.021
40. I. K. Konstantinou, T. A. Albanis, *Appl. Catal. B: Environ*. **2004**, *49*, 1–14. http://dx.doi.org/10.1016/j.apcatb.2003.11.010

Povzetek

Tekom raziskav smo preučevali fotokatalitičen razpad monoazo (metiloranž) in diazo (kongo rdeče) barvil v vodnih raztopinah nanokompozitov Fe^{3+}/C/S dopiranega TiO_2. Nanokompozite smo sintetizirali s sol-gel metodo in karakterizirali z naslednjimi tehnikami: XRD, FTIR, SEM, TEM, EDX, BET in UV-Vis. Fotokatalitični razpad barvil smo spremljali pod simulirano vidno svetlobo, uporabili pa smo TiO_2, C/S dopiran TiO_2 in Fe^{3+}/C/S dopiran TiO_2 z različnimi koncentracijami ionov Fe^{3+}. Preučevali smo vpliv katalizatorja, pH-ja raztopine in intenzitete svetlobe. V primeru Fe^{3+}/C/S dopiranega TiO_2 smo opazili zmanjšano vrednost energijske špranje (band gap) in izboljšano aktivnost vidne svetlobe. Glede na fotokatalitično učinkovitost lahko preučevane materiale zapišemo v naslednjem vrstnem redu: TiO_2 < C/S/ dopiran TiO_2 < Fe^{3+}/C/S dopiran TiO_2. Fe^{3+}/C/S dopiran TiO_2 (0.3% Fe^{3+}) je izkazoval najboljše fotokatalitične lastnosti. V primeru monoazo barvila smo opazili višjo stopnjo razpada kot v primeru diazu barvila. Razpad azo barvil se je zmanjšal s povečanjem pH vrednosti od 2 do 12. Zvišanje intenzitete vidne svetlobe je povečalo učinkovitost razpada barvil pod vplivom svetlobe. Opazili smo, da se je barvilo hitreje razbarvalo, kot pa mineraliziralo.